DOI: 10.1002/chem.200900860

Asymmetrical Fluorene[2,3-*b*]benzo[*d*]thiophene Derivatives: Synthesis, Solid-State Structures, and Application in Solution-Processable Organic Light-Emitting Diodes

Chunyan Du,[a, b] Shanghui Ye,[a, b] Jianming Chen,[a, b] Yunlong Guo,[a, b] Yunqi Liu,*[a] Kun Lu,[a, b] Ying Liu,[a, b] Ting Qi,[a] Xike Gao,[a] Zhigang Shuai,[a] and Gui Yu[a]

Abstract: A series of novel asymmetrical fused compounds containing the backbone of fluorene[2,3-*b*]benzo[*d*]-thiophene (FBT) were effectively synthesized and fully characterized. Single-crystal X-ray studies demonstrated that the length of the substituent side chains greatly affects the solid-state packing of the obtained fused compounds. DFT, photophysical, and electrochemical studies all showed that the FBTs have large band gaps, low-lying HOMO energy levels, and therefore good stability toward oxidation. Moreover, the substituents strongly influence the fluorescence properties of the resulting FBT derivatives. The di-*n*-hexyl compound exhibits intense fluorescence in solution with the highest quantum yield of up to 91%. Solution-processed green phosphorescent organic light-emitting diodes with the di-*n*-butyl derivative as the host material exhibited a maximum brightness of 14185 cd m^{-2} and a luminescence efficiency of 12 cd A^{-1}.

Keywords: fused-ring systems · organic light-emitting diodes · solid-state structures · substituent effects · sulfur heterocycles

Introduction

Conjugated materials, which are one of the most investigated classes of advanced materials, have attracted much attention in recent years because of their potential applications in electronics, photonics, and optoelectronics.[1–4] In contrast to conjugated polymers, conjugated oligomers are characterized because of their well-defined structures and superior chemical purity.[5,6] Among these, ladder-type fused molecules have been the focus of research interest because of their enhanced degree of π-conjugation, highly efficient photoluminescence, and remarkable charge mobility.[7,8] The physical properties of the ladder-type fused molecules can be tailored by changing the degree of conjugation through different backbone units or incorporating heteroatoms, such as sulfur, selenium, phosphorus, nitrogen, and oxygen, as bridging atoms.[9–11] Furthermore, these modifications can also significantly influence their organization in the solid state.[12] The solid-state morphology of organic semiconductors plays an important role in the characteristics of organic electronic devices. Both exciton migration and carrier mobility strongly depend on the solid-state stacking of the conjugated materials. In general, great intermolecular overlap, thus strong electronic interactions, between the adjacent molecules leads to high charge mobility. As we know, the incorporation of heteroatoms would lead to a variety of intra- and intermolecular interactions, such as van der Waals interactions, π–π stacking, and heteroatom interactions, thus affecting not only the electronic structures but also the solid-state structures.[13,14] However, there are still no definite guidelines for molecular design to combine high performance with easy preparation. It is still a major challenge to understand the relationship between molecular structure and properties.

Electrophosphorescent organic light-emitting diodes (OLEDs) with the potential to offer 100% internal efficiencies because they can use both the singlet and triplet excitons for emission have been rapidly developed in recent

[a] C. Du, S. Ye, J. Chen, Y. Guo, Prof. Dr. Y. Liu, K. Lu, Y. Liu, Dr. T. Qi, Dr. X. Gao, Prof. Dr. Z. Shuai, Prof. Dr. G. Yu
Beijing National Laboratory for Molecular Sciences
Organic Solids Laboratory, Institute of Chemistry
Chinese Academy of Sciences, Beijing 100190 (China)
Fax: (+86) 10-62559373
E-mail: liuyq@iccas.ac.cn

[b] C. Du, S. Ye, J. Chen, Y. Guo, K. Lu, Y. Liu
Graduate School of the Chinese Academy of Sciences
Beijing 100190 (China)

Supporting information for this article is available on the WWW under http://dx.doi.org/10.1002/chem.200900860.

years.[15] The way to realize efficient electrophosphorescent OLEDs is to choose suitable host materials that allow for exothermic energy transfer between a host excited state and a lower-energy guest unoccupied orbital, which in turn results in an energetically favorable excited-state transition between molecules.[15] The reported host materials are mostly bulky and sterically hindered molecules, and no fused planar molecules have been reported as host materials in phosphorescent OLEDs.

Fluorene-based materials have been widely studied for their unique optoelectronic properties.[16–18] At present, we find that the studies have mainly focused on polyfluorene[19] and oligomers.[20] Until now, there have only been a few linear fused-ring compounds with the introduction of the fluorene substructure,[21] which may be due to the lack of efficient synthetic strategies. The introduction of fluorene would have a great influence on the solid-state stacking and electronic structure of the compounds, as the C9 position of the fluorene unit could be readily functionalized with a variety of groups. However, how the substituent side chains affect the solid-state structure and the physicochemical properties are still ambiguous.[22] To the best of our knowledge, the introduction of the fluorene substructure in an asymmetrical linear fused-ring molecule has not been reported yet. We recently reported the synthesis and characterization of an asymmetrical heteroacene anthra[2,3-*b*]benzo[*d*]thiophene (ABT).[23] Expanding on our previous work, we have focused on the synthesis and structure–property relationship of asymmetrically substituted fluorene[2,3-*b*]benzo[*d*]thiophene (FBT) compounds. Herein, we have designed and synthesized a series of asymmetrically substituted compounds **4a–d** (see Scheme 1), in which a fluorene unit is fused with benzothiophene, that is, fluorene[2,3-*b*]benzo[*d*]-thiophene, motivated by the aforementioned characteristics. Accordingly, a detailed investigation of the photophysical properties and single-crystal structural studies of substituted FBT is presented to fully explore the influence of different substituents on the inherent electronic properties and solid-state packing arrangement. Furthermore, we prepared a series of solution-processable phosphorescent OLEDs containing FBTs as the host materials for the dopant $[Ir(ppy)_3]$ (ppy = phenylpyridine) to evaluate the application of the FBTs in OLEDs. To the best of our knowledge, this type of fused compound bearing the thiophene ring used as the host material of phosphorescent OLEDs has been rarely described. Herein, we report a flexible molecular design that satisfies the demand for phosphorescent devices.[24]

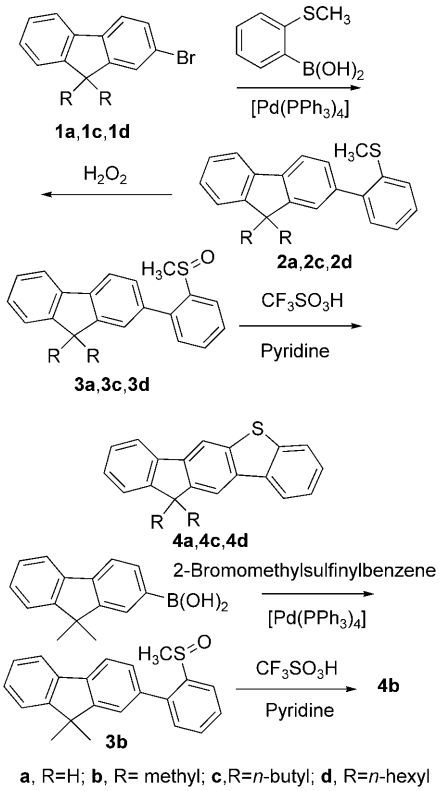

Scheme 1. Synthesis of **4a–d**.

Results and Discussion

Synthesis: The synthesis of the FBTs was conducted with the acid-induced condensation of aromatic methyl sulfoxide groups as a key reaction, which has been used extensively for the preparation of high-molecular-weight polymers and thiophene-based heteroacenes.[25,26] First, the substrates for the condensation were synthesized as shown in Scheme 1. The Suzuki–Miyaura cross-coupling reaction between 9,9-dimethyl-2-fluoreneboronic acid and 2-bromo(methylsulfinylbenzene) produces **3b** in 80% yield. Methyl-substituted FBT **4b** was obtained by treating **3b** with trifluoromethanesulfonic acid for 12 h and subsequent demethylation in water/pyridine. Compounds **4a**, **4c**, and **4d** were synthesized by using a slightly different route because the corresponding fluoreneboronic acids were not commercially available. Compounds **1a**, **1c**, and **1d** were coupled with (2-methylsulfanyl)benzeneboronic acid by using the Suzuki–Miyaura cross-coupling reaction to afford 2-(2-methylsulfanylphenyl)-9,9-dialkylfluorene derivatives **2a**, **2c**, and **2d**. The oxidation of **2a**, **2c**, and **2d** with hydrogen peroxide gave rise to the key 2-(2-methylsulfinylphenyl)-9,9-dialkylfluorene precursors **3a**, **3c**, and **3d**. The final compounds **4a**, **4c**, and **4d** were obtained by treating **3a**, **3c**, and **3d** in a similar procedure to **3b**. As expected, the solubility of the FBTs **4a–d** increases as a function of the length of the alkyl chains. Furthermore, all these compounds exhibit good solubility in common solvents, such as petroleum ether, ethyl acetate, and dichloromethane, thus enabling ready purification by column chromatography and device fabrication with solution processing.

Theoretical calculations for 4a–d: To obtain further insight into the molecular structure and electron distribution and to estimate the position of the frontier orbitals of **4a–d**, DFT

calculations were performed by using Gaussian 03 at the B3LYP/6–31G(d) level. For **4b–d**, the optimized structures are similar to those obtained by X-ray crystallographic studies. The HOMOs and LUMOs for each molecule are spread out over the entire FBT backbone, without localized frontier orbitals. However, with the increase in the length of the alkyl chains at the C9 position of fluorene, the electron density located on the sulfur atoms increased greatly from **4a** to **4d** (Figure 1). The energy values of the HOMO (E_{HOMO}) and LUMO (E_{LUMO})orbitals of **4a–d** were calculated by DFT studies to be $E_{HOMO} = -5.58$, -5.57, -5.56, and -5.55 eV; $E_{LUMO} = -1.24$, -1.26, -1.25, and -1.25 eV; and $E_g = 4.34$, 4.31, 4.31, and 4.30 eV for **4a–d**, respectively.

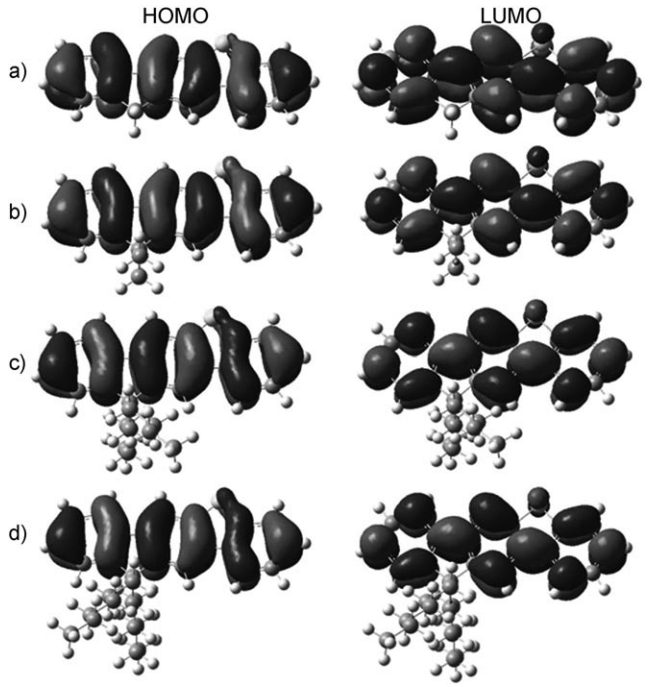

Figure 1. HOMO and LUMO for **4a–d** according to DFT calculations at the B3LYP/6–31G(d) level.

Solid-state structures of 4b–d: Recent studies have shown that the solid-state morphology of conjugated materials plays an important role in the performance characteristics of electronic devices;[1a,2b] thus, X-ray diffraction studies were performed on crystals of **4b–d** to determine their solid-state order and the effect of the side-chain substitution on the solid-state structures. Compound **4b**, obtained as colorless plate crystals upon evaporation from CH_2Cl_2, crystallizes in the orthorhombic system space group *Pca*2(1).[27] The structure of **4b** reveals a nearly planar molecular conformation with the two methyl substituents arranged vertically around the backbone. The compound has π-stacked packing in two dimensions and forms a layer-by-layer solid structure along the *c* axis (see Figure S1 in the Supporting Information). There are three types of short C–H···π contacts between adjacent molecules within each layer of **4b** (Figure 2).

Single crystals of di-*n*-butyl-substituted **4c**, obtained from the slow evaporation of hexane, crystallizes in the triclinic system space group $P\bar{1}$. Compound **4c** has two independent molecules in one unit cell and each molecule possesses an asymmetrical geometry with the two *n*-butyl substituents arranged vertically around the backbone at one side (see Figure 3 and Figure S2 in the Supporting Information). Interestingly, the two *n*-butyl substituents in each molecule were arranged in a different manner with the four carbon atoms of one *n*-butyl substituent adopting a mean '*anti*' geometry and the other a '*syn*' geometry (Figure 3). This arrangement may be because of the steric hindrance of the two molecules in one unit cell. From the stacking structure shown in Figure 3b, we can see that the two independent molecules construct two types of stacking columns arranged in a face-to-face fashion. Two types of short C–H···π contacts (i.e., 2.85 and 2.83 Å, respectively; Figure 3a and 3b) exist between the two independent molecules. The two adjacent molecules in a stacking column are almost parallel, and there are intermolecular C···C interactions (3.34 and 3.35 Å, respectively; Figure 3c and 3d) that exist between adjacent molecules in each column. Besides, the third type of short C–H···π contact (2.80 Å; Figure 3) was observed between two face-to-face molecules in the two columns. As for the pendant *n*-butyl chains, short C–H···C contacts exist between the *anti n*-butyl chain of one molecule and the *syn*

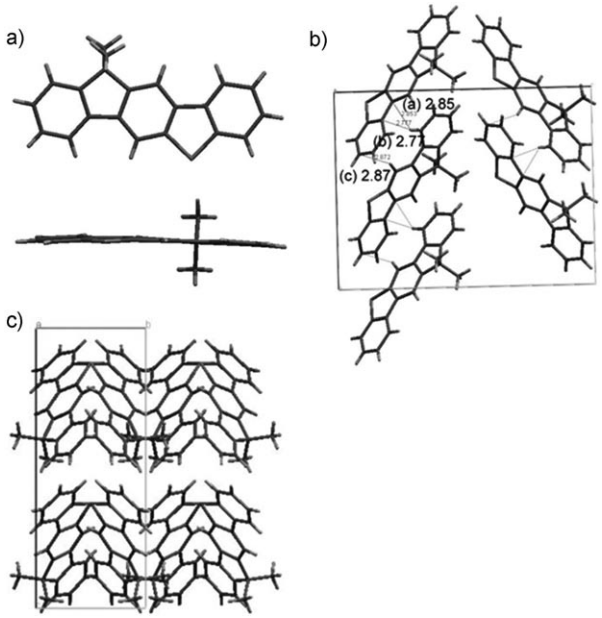

Figure 2. a) Molecular structure of **4b** in the solid state. b) Stacking diagram of **4b** that shows C–H···π hydrogen bonds in the solid state and all the values are given in Å. c) Layer structure packing of **4b** viewed along the *a* axis.

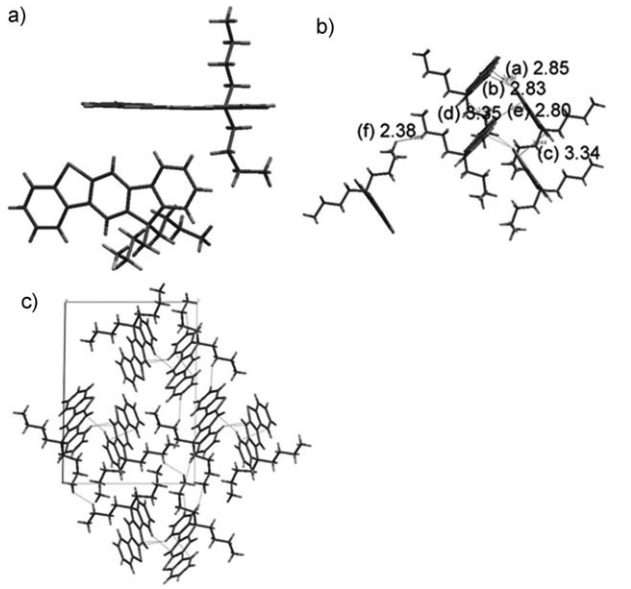

Figure 3. a) Molecular structure of **4c** in the solid state. b) Stacking diagram of **4c** that shows π–π interactions and C–H···π hydrogen bonds in the solid state and all the values are given in Å. c) Crystal packing of **4c** viewed along the *a* axis.

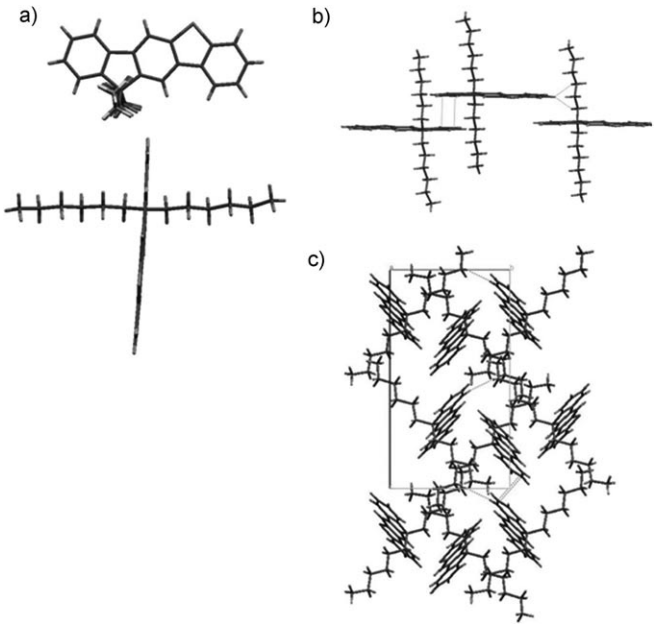

Figure 4. a) Solid-state structure of **4d**, top view and side view. b) Stacking diagram of **4d** that shows π–π interactions and C–H···π hydrogen bonds. c) Crystal packing of **4d** viewed along the *a* axis.

chain of another (Figure 3), which may explain why the two *n*-butyl chains adopt different arrangements.

Di-*n*-hexyl-substituted **4d**, obtained from methanol/dichloromethane at −20 °C, crystallizes in the monoclinic system space group *P*21/*n*. Compound **4d** has a single molecule in one unit cell and possesses a different packing structure from **4b** and **4c**, although these compounds have the same backbone structure (see Figure 4 and Figure S3 in the Supporting Information). The central FBT core was flat and the two *n*-hexyl substituents were arranged almost vertically around the plane of the backbone, with the carbon atoms in both substituents in a mean *anti* geometry. We observed that short C–C contacts (i.e., 3.37 Å) exist between neighboring conjugated planes and that short C–H···π intermolecular interactions exist between the pendant *n*-hexyl chain and the conjugated plane (2.37 Å), which result in the formation of stacking columns in an edge-to-face fashion (see the packing structure shown in Figure 4).

These very different solid-state structures of the three relatives of the same FBT family nicely illustrate how the effect of the substituents can efficiently be utilized to tune the organization in the solid-state of organic semiconductors. Even the simplest variations, such as lengthening the side chain from one to four–six carbon atoms, have tremendous impact on the packing motif of the compound. Further research would yield complementary and useful information in the study of structure–property relationships in organic semiconductors.

Thermal properties: Differential scanning calorimetry (DSC) studies of **4a–d** revealed that these compounds showed decreased melting points (i.e., 240, 183, 120, and 58 °C respectively) with lengthening alkyl chain probably because longer alkyl substitution largely increases the degree of freedom of the FBTs (see Figure S4 in the Supporting Information). However, the thermal decomposition temperature of **4a–d** ($T_d \approx 300$ °C) increased on the order **4b** < **4c** < **4a** < **4d**, as shown by thermogravimetric analysis (TGA; see Figure S4 in the Supporting Information), thus indicating that **4d**, with the longest side chain, has the best thermal stability.

Optical properties: The photophysical properties of FBTs **4a–d** are shown in Figure 5 and Table 1 (also see Figure S5 in the Supporting Information). For the series of FBTs, **4a** without substituents showed a much weaker absorption intensity at long wavelengths than **4b–d**. With the introduction of substituent chains, the absorption maxima of **4a–d** exhibited a slight red shift from 341 to 346 nm. However, for the substitued FBT derivatives **4b–d**, the variations in the absorption spectrum in a dilute solution are much less pronounced, thus indicating that the length of the alkyl chains has no significant effect on the absorption spectrum of the FBTs. In comparison to those spectra recorded in solution, red shifts of $\delta\lambda = 12$, 6, and 9 nm in the absorption maxima for pristine films of **4a**, **4b** and **4c**, and **4d**, respectively, were observed, thus suggesting that moderate intermolecular interactions were present in the solid-state.

The FBTs all exhibited intensive fluorescence both in solution and in the solid state. For **4a**, the solid-state fluorescence emission wavelength maximum is observed at $\lambda_{max} =$ 398 nm and exhibits a red shift of about 34 nm from solution (i.e., 364 nm), which is indicative of strong intermolecular interactions, likely through π stacking. Compounds **4b–d** ex-

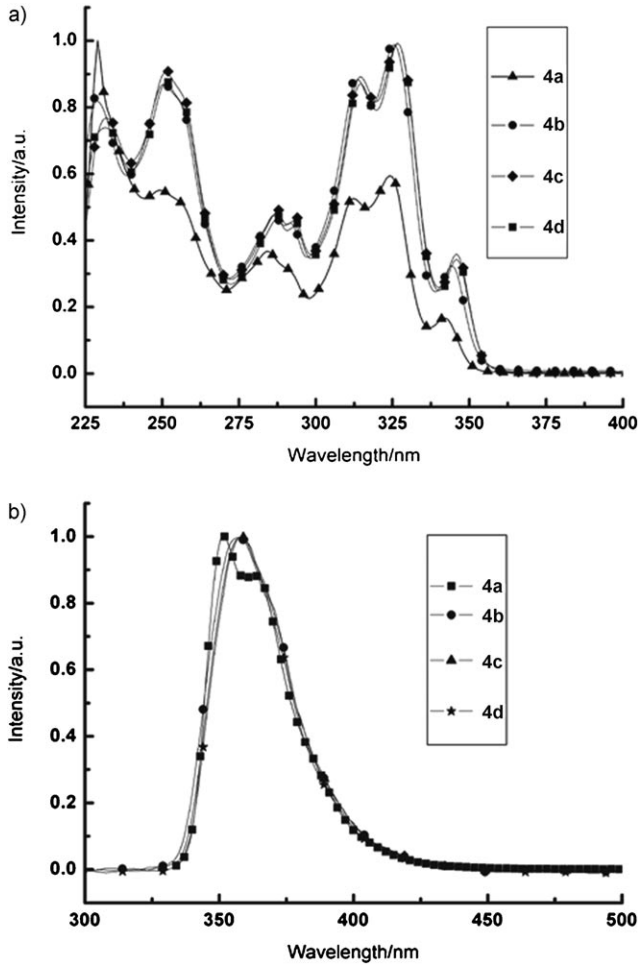

Figure 5. a) Absorption and b) emission spectra of **4a**–**d** in CH_2Cl_2.

Table 1. Photophysical data of **4a**–**d**.

Compound	Solution				Film[e]		
	λ_{abs}[a] [nm]	λ_{lum}[b] [nm]	E_g[c] [eV]	ϕ_f[d]	λ_{abs} [nm]	λ_{lum}[b] [nm]	E_g[c] [eV]
4a	341	351, 364	3.51	0.28	353	398	2.83
4b	344	357	3.48	0.50	350	371	3.06
4c	346	358	3.47	0.78	352	382	3.03
4d	346	359	3.47	0.91	355	365	2.65

[a] Absorption maxima measured in a dilute solution of CH_2Cl_2. [b] Excited at the absorption wavelength maximum. [c] Estimated from the onset of absorption ($E_g = 1240\ eV\lambda_{onset}^{-1}$). [d] Measured in solution with CH_2Cl_2 with naphthalene[28] as a standard at room temperature. [e] Films were drop-cast using a solution of CH_2Cl_2 on a quartz substrate.

hibit similar fluorescence spectra in solution with the wavelength maxima at $\lambda_{max} = 357$, 358, and 359 nm, respectively. But the thin-film fluorescence emissions of **4b**–**d** exhibit different red shifts with the wavelength maximum at $\lambda_{max} = 71$, 382, and 365 nm, respectively. As for **4d**, the fluorescence emission in the thin film shows only a small red shift relative to that of the others, which may be attributed to the fact that **4d** has the longest alkyl chains, which are arranged vertically around the backbone plane and preclude π stacking in the solid state.

Fluorescence quantum yields were determined by using standard procedures with naphthalene ($\phi_f = 0.23 \pm 0.02$)[28] as a reference. Fluorescence quantum yields in dichloromethane were 0.28, 0.50, 0.78, and 0.91 for **4a**–**d**, respectively. The fluorescence quantum yields increase with lengthening of the alkyl substituents, and **4d**, with *n*-hexyl substituents, appears to be significantly more highly fluorescent with the highest quantum yield of 0.91. It is worth noting that the Stokes shift of the fluorescence band of **4a** in the solid state was higher than that of **4b**–**d** (i.e., 45 versus 21, 30, and 30 nm, respectively), thus indicating there are different structural variations between the excited and ground states.

Relative to indenofluorene (IF),[29] the absorption spectrum wavelength maximum of **4a** showed a red shift of $\delta\lambda = 7$ nm from $\lambda_{max} = 333$ of IF[29] to 341 nm of **4a** in solution, and the optical gap estimated from the absorption edges of the solution spectra for **4a** is 3.51 eV, which is smaller than that of IF (i.e., 3.71 eV). The structural difference between **4a** and IF is that the indene unit in IF was changed to the benzothiophene unit in **4a**, thus resulting in spectral change and demonstrating that the introduction of the π-electron-rich thiophene moiety impacts greatly on the optical properties.

Cyclic voltammetry: The electrochemical stabilities of FBTs were investigated by cyclic voltammetry (CV), and the electrochemical characteristics are listed in Table 2. For **4a**, a quasi-reversible oxidation wave was observed and the oxidation peak maximum was 1.54 eV. However, **4b**–**d** showed two quasi-reversible oxidation waves (see Figure S6 in the Supporting Information) and the first oxidation peaks maxima of **4a**–**d** were +1.59, +1.57, and +1.54 V versus A_g/A_gCl, respectively. The HOMO levels (E_{HOMO}) of **4a**–**d** were estimated from the first oxidation onsets to be −5.84, −5.84, −5.83, and −5.83 eV, respectively, which are much lower

Table 2. Cyclic voltammogram data[a] and optical band gaps of **4a**–**d** and IF for comparison.

Compound	**4a**	**4b**	**4c**	**4d**	IF[g]
E_{ox}^{peak} [eV]	1.54	1.59, 1.75[f]	1.57, 1.76[f]	1.54, 1.73[f]	1.25
E_{HOMO} [eV][b]	−5.58	−5.57	−5.56	−5.55	−5.43
E_{HOMO} [eV][c]	−5.84	−5.84	−5.83	−5.83	−5.65
E_{LUMO} [eV][b]	−1.24	−1.26	−1.25	−1.25	−1.13
E_{LUMO} [eV][d]	−2.33	−2.36	−2.36	−2.36	−1.94
E_g[e] [eV]	3.51	3.48	3.47	3.47	3.71

[a] Performed in a solution of Bu_4NPF_6 in CH_3CN; $\nu = 100\ mV\,s^{-1}$. [b] Calculated through DFT studies. [c] Obtained according to UV/Vis spectra by using the empirical equation: $E_{HOMO} = -(4.4 + E_{ox}^{onset})$. [d] Calculated from the E_g and E_{HOMO} values. [e] Estimated from the onset of absorption in CH_2Cl_2 ($E_g = 1240\ eV\lambda_{onset}^{-1}$). [f] Second oxidation. [g] From ref. [29].

than that of indenofluorene (−5.65 eV)[29a] and other reported fused compounds that incorporate a sp^3 carbon atom as a carbon bridge[30] and are indicative that FBTs are more stable under ambient conditions. Based on the HOMO levels and the optical-band gaps evaluated from the onset wavelength of the UV/Vis absorption spectra, LUMO energy levels of the FBTs were calculated to be $E_{LUMO} = -2.33$ and −2.36 eV for **4a** and **4b–d**, respectively. As compared with IF, changing indene with the benzothiophene unit in FBTs has a large influence on the HOMO and LUMO energy levels because of the heteroatom effectiveness[13,14] of the thiophene unit. However, the length of the alkyl chains has little effect on the energy levels, thus leaving the HOMO and LUMO energy levels almost unchanged from **4b** to **4d**.

Device fabrication of OLEDs: To explore the application of the FBTs in OLEDs, we investigated the use of FBTs as the host material and $[Ir(ppy)_3]$ as the emitter for green phosphorescent devices, with the device structure of indium tin oxide (ITO)/polyethylene dioxythiophene–polystyrene sulfonate (PEDOT–PSS; 30 nm)/**4a–d**: (w, 10%), $[Ir(ppy)_3]$ (45 nm)/2,9-dimethyl-4,7-diphenyl-1,10-phenanthroline (BCP; 40 nm)/Ca–Ag (100 nm). The conducting polymer PEDOT–PSS was used as the hole injection layer. The emitting layer consisted of **4a–d** doped with 10 wt% of green phosphor $[Ir(ppy)_3]$. BCP was used as a hole-blocking layer. In the electroluminescence and film spectra ($\lambda_{max} = 514$ and 510 nm) of 10% $[Ir(ppy)_3]$ in **4a–d**, only $[Ir(ppy)_3]$ emissions were observed from the device, thus indicating complete energy transfer to the phosphorescent dopant from the FBTs. All the devices exhibited green-light emission with a peak centered at $\lambda = 514$ nm and Commission International de L'Eclairage (CIE) 1931 chromaticity coordinates of (0.32, 0.61). Figure 6 displays the current density/voltage/luminance and luminance efficiency/luminance characteristics of the devices with different host materials **4a–d**. The best performance was achieved for the device when using **4c** as the host material with a maximum luminance of 14185 cd m^{-2} at 18 V and a luminance efficiency of 12 cd A^{-1} at the luminance of 600 cd m^{-2}. The luminance efficiencies of the devices fabricated with **4b** and **4d** are 1.2 and 2.8 cd A^{-1}, respectively, which are lower than that of **4c** but much higher than that of **4a** (0.05 cd A^{-1}). Devices based on **4d** exhibit a lower performance with a luminance of 2155 cd m^{-2} at 13 V. The poor performance of **4a** and **4b** may be attributed to their solid structure because they have short substituents at the C9 position of fluorene, thereby forming densely packed solid structures that readily induce fluorescence quenching. As we know, a suitable host material in the phosphorescent OLEDs must have limited conjugation length, and thus rather large energy gaps to prevent reverse energy transfer from the guest back to the host and confine triplet excitons on the guest molecules.[31] For fused small molecules used as host materials and devices fabricated with simple spin-coating deposition, our results are comparable to the best performance. With further modification of the FBTs and optimization of the device structures, these materials may prove to be excellent host materials for future OLED display applications.

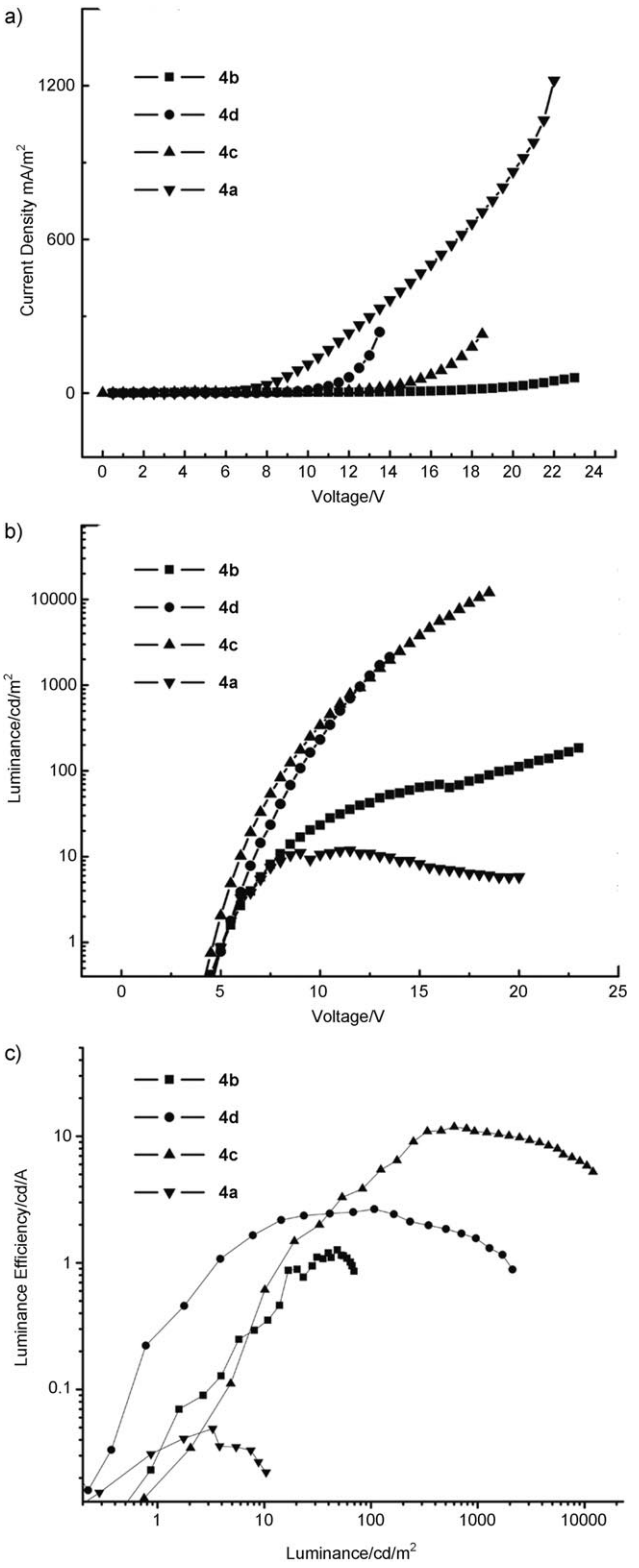

Figure 6. a) Current density/voltage, b) luminance/voltage and c) luminance efficiency/luminance of the devices with **4a–d**.

Conclusions

In conclusion, we have reported the synthesis and properties of asymmetrical FBT derivatives. To the best of our knowledge, this report is the first of core asymmetrical ladder-type fused molecules that incorporate fluorene and thiophene units simultaneously. The FBTs are soluble in common organic solvents and exhibit different packing with different lengths of alkyl substituents in the solid state. Fluorescence spectra show that all the FBTs exhibit intense fluorescence in solution with quantum yields of up to 0.91 for di-*n*-hexyl-substituted **4d**. DFT, photophysical, and electrochemical studies suggest that FBTs have low-lying HOMO levels and thus higher oxidative stability than most fused-ring compounds. Preliminary results of OLEDs with FBTs indicate that the FBTs are promising host materials that perform very efficiently and have low fabrication costs for further OLED applications. Furthermore, the effect of the substituents can be efficiently utilized to tune the solid-state structure and electronic properties of organic semiconductors, which is a powerful method for obtaining semiconducting materials with a variety of desirable attributes.

Experimental Section

Instruments and measurement: ^{1}H NMR (400 MHz) spectra were obtained on a Bruker DMX-400 NMR spectrometer with tetramethylsilane (TMS) as an internal standard. High-resolution mass spectrometry (HRMS) and EIMS were carried out on a Micromass GCT-MS spectrometer. Elemental analyses were performed on a Carlo Erba model 1160 elemental analyzer. Electronic absorption spectra were measured on a Jasco V570 UV/Vis spectrophotometer. TGA-differential thermal analysis (DTA) measurements were carried out on a TA SDT 2960 instruments under a dry nitrogen flow with heating from room temperature to 500 °C at a heating rate of 10 °C min^{-1}. Cyclic voltammetric measurements were carried out in a conventional three-electrode cell using Pt button working electrodes 2 mm in diameter, a platinum wire counterelectrode, and a Ag/AgCl reference electrode on a computer-controlled CHI660C instrument at room temperature. X-ray diffraction studies were carried out in the reflection mode at room temperature on a 2-kW Rigaku X-ray diffraction system.

OLED fabrication and characterization: All the OLEDs were fabricated on bare ITO substrates that were cleaned with detergent, deionized water, acetone, and ethanol. Films of PEDOT–PSS were spin-cast onto precleaned ITO substrates. A mixture of [Ir(ppy)$_3$] and host materials (10 wt %) was spin-cast from a solution in $CHCl_3$. A Newport 2835-C multifunction optical meter was used to measure luminance output. Current/voltage characteristics were measured with a Hewlett–Packard 4140B semiconductor parameter analyzer. CIE coordinates were measured with a PhotoResearch PR-650 spectrophotometer.

Single-crystal X-ray analysis of 4b–d: The measurements of **4b–d** were made on a diffractometer with $Mo_{K\alpha}$ radiation ($\lambda = 0.71073$ Å) at 113(2) K. The structures were solved and defined by direct methods and SHELXS-97. The hydrogen atoms were located at the calculated positions. Absorption correction was applied using semiempirical measurements from equivalents.

4b: $C_{21}H_{16}S$, $M_r = 300.40$, colorless plates, crystal size $0.40 \times 0.38 \times 0.12$ mm; orthorhombic, space group *Pca*2(1); $a = 13.522(3)$, $b = 6.8691(14)$, $c = 17.579(4)$ Å; $\alpha = 90.00$, $\beta = 90.00$, $\gamma = 90.00°$; $V = 1632.8(6)$ Å^3; $Z = 4$, $\rho_{calcd} = 1.222$ g cm^{-3}; $\mu = 0.192$ mm^{-1}; $T = 113(2)$ K; 2812 data (1618, $R_{int} = 0.1383$, $2.32 \le \theta \le 25.02$); GOF = 0.971; 202 parameters; $R = 0.0793$.

4c: $C_{27}H_{28}S$, $M_r = 384.55$, colorless plates, crystal size $0.20 \times 0.18 \times 0.16$ mm; triclinic, space group $P-1$; $a = 8.5753(12)$, $b = 13.6692(15)$, $c = 18.691(2)$ Å; $\alpha = 90.557(5)$, $\beta = 91.676(7)$, $\gamma = 98.547(4)°$; $V = 2165.4(4)$ Å^3, $Z = 4$, $\rho_{calcd} = 1.180$ g cm^{-3}; $\mu = 0.159$ mm^{-1}; $T = 113(2)$ K; 9268 data (6428, $R_{int} = 0.0423$, $1.87 \le \theta \le 27.28$); GOF = 1.073; 509 parameters; $R = 0.0423$.

4d: $C_{31}H_{36}S$, $M_r = 440.66$, colorless plates, crystal size $0.16 \times 0.14 \times 0.10$ mm; monoclinic, space group *P*21/*n*; $a = 12.247(2)$, $b = 10.708(2)$, $c = 19.793(4)$ Å; $\alpha = 90.00$, $\beta = 99.63(3)$, $\gamma = 90.00°$; $V = 2559.1(9)$ Å^3, $Z = 4$, $\rho_{calcd} = 1.144$ g cm^{-3}; $\mu = 0.142$ mm^{-1}; $T = 113(2)$ K; 4502 data (3842, $R_{int} = 0.0556$, $2.13 \le \theta \le 25.02$); GOF = 1.099; 291 parameters; $R = 0.0355$.

Synthesis of 2-(2-methylsulfanylphenyl)-9,9-di-*n*-butylfluorene (2c): K_2CO_3 solution (2 M, 15 mL) was added to a mixture of **1c** (1.16 g, 3 mmol) and 2-methylsulfanylbenzeneboronic acid (0.504 g, 3 mmol) in freshly distilled toluene (20 mL) under argon. [Pd(PPh$_3$)$_4$] (100 mg) was the added in one portion to the reaction mixture, which was heated to reflux for 24 h. The mixture was cooled to room temperature and extracted with ethyl acetate. The organic layers were dried, evaporated in vacuum, the residue was purified by column chromatography on silica gel with petroleum ether as the eluent to give pure **2c** as a white solid (1 g, 83 %). MS (EI): *m*/*z* (%): 400 [*M*$^+$]; ^{1}H NMR (400 MHz, $CDCl_3$): $\delta =$ 0.82–0.85 (m, 10H), 1.22–1.27 (m, 4H), 2.13–2.18 (m, 4H), 2.44 (s, 3H), 7.44–7.53 (m, 8H), 7.64 (s, 1H), 7.85–7.90 ppm (m, 2H); ^{13}C NMR (400 MHz, $CDCl_3$): $\delta = 14.20$, 16.32, 23.44, 26.34, 40.48, 55.35, 119.76, 120.08, 123.14, 124.58, 125.13, 125.92, 127.11, 127.38, 128.10, 128.17, 130.35, 137.64, 139.55, 140.77, 141.21, 141.90, 150.69, 151.35 ppm; elemental analysis calcd (%) for $C_{28}H_{32}S$: C 83.95, H 8.05; found: C 83.58, H 8.07.

Synthesis of 2-(2-methylsulfinylphenyl)-9,9-dimethylfluorene (3b): K_2CO_3 solution (2 M, 15 mL) was added to a mixture of 9,9-dimethyl-2-fluoreneboronic acid (1.19 g, 5 mmol) and 2-bromo(methylsulfinyl)benzene (1.1 g 5 mmol) in freshly distilled toluene (20 mL) under argon. [Pd(PPh$_3$)$_4$] (100 mg) was added in one portion to the reaction mixture, which was heated to reflux for 24 h. The mixture was cooled to room temperature and extracted with ethyl acetate. The organic layers were dried, evaporated in vacuum, and the residue was purified with column chromatography on silica gel with petroleum ether/ethyl acetate (2:1) as the eluent to give pure **3b** as a pale-white solid (1.3 g, 80 %). MS (EI): *m*/*z* (%): 332 [*M*$^+$]; ^{1}H NMR (400 MHz, $CDCl_3$): $\delta = 1.49$ (s, 3H), 1.55 (s, 3H), 2.36 (s, 3H), 7.32–7.34 (d, 1H), 7.35–7.38 (t, 2H), 7.40–7.42 (d, 1H), 7.45–7.48 (m, 2H), 7.55–7.59 (t, 1H), 7.61–7.65 (t, 1H), 7.75–7.80 (m, 2H), 8.13–8.16 ppm (d, 1H); ^{13}C NMR (400 MHz, $CDCl_3$): $\delta = 27.05$, 41.44, 46.97, 120.25, 120.33, 122.70, 123.43, 123.56, 127.16, 127.78, 127.97, 128.60, 130.31, 130.65, 136.64, 138.30, 139.39, 139.84, 143.98, 153.75, 154.24 ppm; elemental analysis calcd (%) for $C_{22}H_{20}OS$: C 79.48, H 6.06; found: C 79.23, H 6.12.

Synthesis of 2-(2-methylsulfinylphenyl)-9,9-di-*n*-butylfluorene (3c): Hydrogen peroxide (35 %, 0.25 g) dissolved in glacial acetic acid (10 mL) was added dropwise to **2c** (2.5 mmol, 1 g) dissolved in glacial acetic acid (60 mL). The reaction mixture was allowed to stir at room temperature for 6 h. The acetic acid was removed by evaporation under vacuum and the crude product was purified with column chromatography on silica gel with petroleum ether/ethyl acetate (2:1) as the eluent to afford **3c** as a colorless oil (0.95 g, 92 %). MS (EI): *m*/*z* (%): 416 [*M*$^+$]; ^{1}H NMR (400 MHz, $CDCl_3$): $\delta =$ 0.51–0.63 (m, 8H), 0.76–1.13 (m, 6H), 1.86–1.96 (m, 4H), 2.25 (s, 3H), 7.20–7.27 (m, 4H), 7.30–7.32 (m, 2H), 7.42–7.47 (t, 1H), 7.49–7.53 (t, 3H), 7.62–7.64 (m, 1H), 7.66–7.68 (d, 1H), 8.04–8.06 ppm (d, 1H); ^{13}C NMR (400 MHz, $CDCl_3$): $\delta = 14.29$, 21.16, 23.15, 26.30, 41.12, 55.38, 120.15, 120.36, 123.09, 123.70, 123.77, 127.16, 127.83, 128.00, 128.76, 130.57, 130.89, 136.53, 140.13, 140.39, 141.66, 143.74, 150.99, 151.55 ppm; elemental analysis calcd (%) for $C_{28}H_{32}OS$: C 80.72, H 7.74; found: C 80.81, H 7.91.

Synthesis of 9,9-dimethylfluorene[2,3-*b*]benzo[*d*]thiophene (4b): Compound **3b** (1 g, 3 mmol) was added to trifluoromethanesulfonic acid (4.5 mL). The solution was stirred at room temperature for 24 h and then poured slowly into water/pyridine (90 mL, 8:1). Demethylation was achieved by heating the mixture to reflux for 30 min. Upon cooling, the mixture was extracted with dichloromethane. The organic extracts were washed with brine and dried with M_gSO_4. After removing the solvent by

evaporation, the residue was purified with column chromatography on silica gel with petroleum ether as the eluent to afford **4b** as a white solid (0.72 g, 80%). MS (EI): *m/z* (%): 300 [M^+]; ^{1}H NMR (400 MHz, $CDCl_3$): $\delta = 1.59$ (s, 6H), 7.35–7.38 (m, 2H), 7.43–7.48 (m, 3H), 7.78–7.80 (d, 1H), 7.83–7.84 (d, 1H), 8.16–8.17 (d, 2H), 7.18–8.20 ppm (d, 1H); ^{13}C NMR (400 MHz, $CDCl_3$): $\delta = 27.95$, 46.74, 114.13, 115.67, 120.36, 121.52, 122.98, 123.06, 124.48, 126.54, 127.36, 127.91, 135.06, 135.80, 138.76, 138.83, 139.26, 139.97, 151.08, 154.38 ppm; elemental analysis calcd (%) for $C_{21}H_{16}S$: C 83.96, H 5.37; found: C 83.90, H 5.46.

Synthesis of 9,9-di-*n*-butylfluorene[2,3-*b*]benzo[*d*]thiophene (4c): Compound **4c** was prepared in a procedure similar to **4b**, thus affording **4c** as a white solid (0.72 g, 80%). MS (EI): *m/z* (%): 384 [M^+]; ^{1}H NMR (400 MHz, $CDCl_3$): $\delta = 0.63$–0.67 (m, 10H), 1.05–1.09 (m, 4H), 2.06–2.09 (m, 4H), 7.35–7.36 (m, 3H), 7.41–7.48 (m, 2H), 7.76–7.78 (d, 1H), 7.83–7.86 (d, 1H), 8.07 (s, 1H), 8.14 (s, 1H), 8.20–8.22 ppm (d, 1H); ^{13}C NMR (400 MHz, $CDCl_3$): $\delta = 13.97$, 23.26, 26.16, 40.99, 54.88, 113.82, 115.73, 120.04, 121.59, 123.08, 123.18, 124.44, 126.49, 127.10, 127.72, 134.96, 135.87, 138.62, 139.95, 140.66, 141.20, 148.08, 151.42 ppm; elemental analysis calcd (%) for $C_{27}H_{28}S$: C 84.32, H 7.34; found: C 84.34, H 7.58.

Acknowledgements

We acknowledge financial support from the National Natural Science Foundation of China (20825208, 60736004, 60671047, 50673093, 20721061), the National Major State Basic Research Development Program (2006CB806203, 2006CB932103, 2009CB623603), the National High-Tech Research Development Program of China (2008AA03Z101), and the Chinese Academy of Sciences.

[1] a) J. E. Anthony, *Chem. Rev.* **2006**, *106*, 5028–5048; b) B. S. Ong, Y. Wu, Y. Li, P. Liu, H. Pan, *Chem. Eur. J.* **2008**, *14*, 4766–4778; c) H. E. Katz, Z. Bao, S. L. Gilat, *Acc. Chem. Res.* **2001**, *34*, 359–369.

[2] a) Y. Shirota, H. Kageyama, *Chem. Rev.* **2007**, *107*, 953–1010; b) J. E. Anthony, *Angew. Chem.* **2008**, *120*, 460–492; *Angew. Chem. Int. Ed.* **2008**, *47*, 452–483.

[3] G. S. He, L. S. Tan, Q. Zheng, P. N. Prasad, *Chem. Rev.* **2008**, *108*, 1245–1330.

[4] S. C. Lo, P. L. Burn, *Chem. Rev.* **2007**, *107*, 1097–1116.

[5] a) P. F. H. Schwab, J. R. Smith, J. Michl, *Chem. Rev.* **2005**, *105*, 1197–1280; b) M. Melucci, L. Favaretto, C. Bettini, M. Gazzano, N. Camaioni, P. Maccagnani, P. Ostoja, M. Monari, G. Barbarella, *Chem. Eur. J.* **2007**, *13*, 10046–10054.

[6] A. R. Murphy, J. M. J. Frechet, *Chem. Rev.* **2007**, *107*, 1066–1096.

[7] a) Y. Lin, D. Gundlach, S. Nelson, T. Jackson, *IEEE Trans. Electron Devices* **1997**, *44*, 1325–1331; b) M. A. Wolak, J. Delcamp, C. A. Landis, P. A. Lane, J. Anthony, Z. Kafafi, *Adv. Funct. Mater.* **2006**, *16*, 1943–1949; c) T. Okamoto, K. Kudoh, A. Wakamiya, S. Yamaguchi, *Chem. Eur. J.* **2007**, *13*, 548–556.

[8] a) J. Roncali, *Chem. Rev.* **1997**, *97*, 173–205; b) A. Pietrangelo, M. J. MacLachlan, M. O. Wolf, B. O. Patrick, *Org. Lett.* **2007**, *9*, 3571–3573.

[9] a) M. L. Tang, T. Okamoto, Z. Bao, *J. Am. Chem. Soc.* **2006**, *128*, 16002–16003; b) H. Ebata, E. Miyazaki, T. Yamamoto, K. Takimiya, *Org. Lett.* **2007**, *9*, 4499–4502; c) J. G. Laquindanum, H. E. Katz, A. J. Lovinger, *J. Am. Chem. Soc.* **1998**, *120*, 664–672.

[10] Y. Dienes, M. Eggenstein, T. Karpati, T. C. Sutherland, L. Nyulaszi, T. Baumgartner, *Chem. Eur. J.* **2008**, *14*, 9878–9889.

[11] a) Y. Ma, Y. Sun, Y. Liu, J. Gao, S. Chen, X. Sun, W. Qiu, G. Yu, G. Cui, W. Hu, D. Zhu, *J. Mater. Chem.* **2005**, *15*, 4894–4898; b) K. Kawaguchi, K. Nakano, K. Nozaki, *J. Org. Chem.* **2007**, *72*, 5119–5128.

[12] a) K. Kawaguchi, K. Nakano, K. Nozaki, *Org. Lett.* **2008**, *10*, 1199–1202; b) Y.-C. Chang, Y.-D. Chen, C.-H. Chen, Y.-S. Wen, J. T. Lin, H.-Y. Chen, M.-Y. Kuo, I. Chao, *J. Org. Chem.* **2008**, *73*, 4608–4614.

[13] V. Lemaur, D. A. da Silva Filho, V. Coropceanu, M. Lehmann, Y. Geerts, J. Piris, M. G. Debije, A. M. van de Craats, K. Senthilkumar, L. D. A. Siebbeles, J. M. Warman, J.-L. Bredas, J. Cornil, *J. Am. Chem. Soc.* **2004**, *126*, 3271–3279.

[14] G. Barbarella, M. Zambianchi, A. Bongini, L. Antolini, *Adv. Mater.* **1993**, *5*, 834–838.

[15] a) M. A. Baldo, D. F. O'Brien, Y. You, A. Shoustikov, S. Sibley, M. E. Thompson, S. R. Forrest, *Nature* **1998**, *395*, 151; b) D. F. O'Brien, M. A. Baldo, M. E. Thompson, S. R. Forrest, *Appl. Phys. Lett.* **1999**, *74*, 442.

[16] a) D. Neher, *Macromol. Rapid Commun.* **2001**, *22*, 1365–1385; b) J. Jo, C. Chi, S. Hoger, G. Wegner, D. Y. Yoon, *Chem. Eur. J.* **2004**, *10*, 2681; c) C. Chi, C. Im, V. Enkelmann, A. Ziegler, G. Lieser, G. Wegner, *Chem. Eur. J.* **2005**, *11*, 6833.

[17] X. H. Zhou, Y. Zhang, Y. Q. Xie, Y. Cao, J. Pei, *Macromolecules* **2006**, *39*, 3830–3840.

[18] A. P. Kulkarni, X. Kong, S. A. Jenekhe, *J. Phys. Chem. B* **2004**, *108*, 8689–8701.

[19] B. Pal, W.-C. Yen, J.-S. Yang, C.-Y. Chao, Y.-C. Hung, S.-T. Lin, C.-H. Chuang, C.-W. Chen, W.-F. Su, *Macromolecules* **2008**, *41*, 6664–6671.

[20] a) Z. Wang, H. Shao, J. Ye, L. Zhang, P. Lu, *Adv. Funct. Mater.* **2007**, *17*, 253–263; b) F. Jaramillo-Isaza. M. L. Turner, *J. Mater. Chem.* **2006**, *16*, 83–89; c) H. S. Lee, T. Nakamura, T. Tsutsui, *Org. Lett.* **2001**, *3*, 2005–2007.

[21] a) N Cocherel, C. Poriel, J. R. Berthelot, F. Barriere, N. Audebrand, A. M. A. Slawin, L. Vignau, *Chem. Eur. J.* **2008**, *14*, 11328; b) K.-T. Wong, T.-C. Chao, L.-C. Chi, Y.-Y. Chu, A. Balaiah, S.-F. Chiu, Y.-H. Liu, Y. Wang, *Org. Lett.* **2006**, *8*, 5033–5036.

[22] a) A. S. Paraskar, A. R. Reddy, A. Patra, Y. H. Wijsboom, O. Gidron, L. J. W. Shimon, G. Leitus, M. Bendikov, *Chem. Eur. J.* **2008**, *14*, 10639–10647; b) M. He, F. Zhang, *J. Org. Chem.* **2007**, *72*, 442–451.

[23] C. Du, Y. Guo, Y. Liu, W. Qiu, H. Zhang, X. Gao, Y. Liu, T. Qi, K. Lu, G. Yu, *Chem. Mater.* **2008**, *20*, 4188–4190.

[24] a) M. A. Baldo, S. Lamansky, P. E. Burrows, M. E. Thompson, S. R. Forrest, *Appl. Phys. Lett.* **1999**, *75*, 4–6; b) R. J. Holmes, S. R. Forrest, Y. J. Tung, R. C. Kwong, J. J. Brown, S. Garon, M. E. Thompson, *Appl. Phys. Lett.* **2003**, *82*, 2422–2424.

[25] a) K. Yamamoto, E. Shouji, H. Nishide, E. Tsuchida, *J. Am. Chem. Soc.* **1993**, *115*, 5819–5820; b) E. Tsuchida, E. Shouji, K. Yamamoto, *Macromolecules* **1993**, *26*, 7144–7148; c) L. Wang, T. Soczka-Guth, E. Havinga, K. Müllen, *Angew. Chem.* **1996**, *108*, 1602–1604; *Angew. Chem. Int. Ed. Engl.* **1996**, *35*, 1495–1497; d) J. Leuninger, C. Wang, T. Soczka-Guth, V. Enkelmann, T. Pakula, K. Mullen, *Macromolecules* **1998**, *31*, 1720-.1727; e) J. Leuninger, C. Wang, T. Soczka-Guth, K. Mullen, *Synth. Metals* **1999**, *101*, 681–684.

[26] a) H. Sirringhaus, R. H. Friend, C. Wang, J. Leuninger, K. Müllen, *J. Mater. Chem.* **1999**, *9*, 2095–2101; b) P. Gao, D. Beckman, H. Tsao, X. Feng, V. Enkelmann, W. Pisulaz, K. Mullen, *Chem. Commun.* **2008**, 1548–1550; c) P. Gao, X. Feng, X. Yang, V. Enkelmann, M. Baumgarten, K. Mullen, *J. Org. Chem.* **2008**, *73*, 9207–9213.

[27] The experimental details, characterization of compounds, X-ray crystallographic data, and cyclic voltammetry are provided in the Supporting Information. CCDC-714676 (**4b**), CCDC-707897 (**4c**), and CCDC-702043 (**4d**) contain the supplementary crystallographic data for this paper. These data can be obtained free of charge from The Cambridge Crystallographic Data Centre via www.ccdc.cam.ac.uk/data_request/cif.

[28] I. B. Berlman, *Handbook of fluorescence spectra of aromatic molecules*, Academic Press, New York, **1965**.

[29] a) S. Merlet, M. Birau, Z. Y. Wang, *Org. Lett.* **2002**, *4*, 2157–2159; b) C. Poriel, J. J. Liang, J. Rault-Berthelot, F. Barriere, N. Cocherel, A. M. Z. Slawin, D. Horhant, M. Virboul, G. Alcaraz, N. Audebrand, L. Vignau, N. Huby, G. Wantz, L. Hirsch, *Chem. Eur. J.* **2007**, *13*, 10055–10069.

[30] J. Roncali, C. Thobie-Gautier, *Adv. Mater.* **1994**, *6*, 846–848.

[31] a) K. T. Wong, Y. M. Chen, Y. T. Lin, H. C. Su, C. Wu, *Org. Lett.* **2005**, *7*, 5361–5364; b) I. Avilov, P. Marsal, J. L. Bredas, D. Beljonne, *Adv. Mater.* **2004**, *16*, 1624–1629.

Received: April 2, 2009
Published online: July 16, 2009

